Asymmetric explosion of clusters in intense laser fields

M. Kundu

Citation: Physics of Plasmas **19**, 083108 (2012); doi: 10.1063/1.4747160
View online: http://dx.doi.org/10.1063/1.4747160
View Table of Contents: http://scitation.aip.org/content/aip/journal/pop/19/8?ver=pdfcov
Published by the AIP Publishing

Asymmetric explosion of clusters in intense laser fields

M. Kundu
Institute for Plasma Research, Bhat, Gandhinagar 382 428, Gujarat, India

(Received 25 May 2012; accepted 6 August 2012; published online 21 August 2012)

We examine asymmetric expansion of argon clusters illuminated by 800 nm laser pulses of duration ≈23 fs, using three-dimensional particle-in-cell (PIC) simulation. For this short pulse duration, laser energy absorption by cluster electrons is dominated by the nonlinear resonance (NLR) absorption process [Phys. Rev. Lett. **96**, 123401 (2006)]. In this work, we concentrate, particularly, on the ionic outcome in the NLR regime and show that higher charge states of argon ions are produced along the laser polarization than in the transverse directions leading to the anisotropy (asymmetry) in the ion energy distribution. *This* anisotropy already established during the short pulse duration (or in the early duration of a long pulse) may contribute to the anisotropic ion emission reported in cluster experiments with pulse duration longer than 100 fs. Our PIC results are compared with a charged-sphere model showing that cluster explosion is mainly due to Coulomb repulsion between the cluster ions. © *2012 American Institute of Physics*. [http://dx.doi.org/10.1063/1.4747160]

I. INTRODUCTION

Atomic clusters are known to absorb incident laser radiation very efficiently leading to creation of multiply charged[1–7] energetic ions (e.g., for argon, xenon). Typical size of a cluster being of the order of a few nano-meter, laser light (248-800 nm wavelength) can fully illuminate and penetrate this target of solid-like atomic density leading to the efficient absorption. For laser intensities $<10^{18}$ Wcm^{-2}, ion kinetic energies in the range of a few hundred keV to MeV (Refs. 1–10) have been observed in experiments with clusters. From the application point of view, energetic ions are useful for nuclear fusion (with deuterium clusters) as well as in medical treatment.

The laser-cluster interaction scenario may be understood as follows: After the irradiation of a cluster with intense laser (sufficient to ionize the atoms in the cluster), electrons first absorb energy and leave their parent ions which is called "inner ionization." A fraction of these electrons will completely leave the cluster (known as "outer ionization") by the combined action of the laser field and the space charge field. Due to "outer ionization" space charge field increases further and the resulting field may create even higher charge states. This enhanced ionization is known as "ionization ignition"[11–19] which may continue until the restoring force of ions on the electrons becomes higher than the applied laser field. The ion dynamics that evolve simultaneously, and continue for a longer time (even after the pulse is switched off) is the direct consequence of outer ionization and the mechanism behind it.

We ignore collisional processes which were reported less significant for wavelengths ≥800 nm (Refs. 16–19) whereas at shorter wavelengths[19–21] those may be important. In the collisionless regime, two different resonance mechanisms of energy absorption exist. The first one of these is the well known "linear resonance" (LR) absorption[22–30] which occurs when time dependent Mie-frequency $\omega_{\mathrm{Mie}}(t)$ of the expanding cluster meets the laser frequency ω with a longer pulse duration, typically >100 fs. This LR is manifested by a peak in the absorption curve,[22] provided ionic charge density remains uniform. On the other hand, for a short pulse (or early cycles of a long pulse) LR does not occur because expansion of cluster is not sufficient to satisfy the condition $\omega_{\mathrm{Mie}}(t) = \omega$, but electrons can absorb energy efficiently through the nonlinear resonance (NLR).[31–33] During NLR, the time dependent eigen frequency $\Omega(t)$ of a laser-driven electron in the anharmonic potential satisfies $\Omega(t) = \omega$. In fact, experiments[34] with 28 fs laser pulses (of wavelength 820 nm) reported nearly 80% laser energy absorption with rare-gas clusters at an intensity 10^{17} Wcm^{-2} while only 25% absorption for the intensity below 10^{16} Wcm^{-2}. This intensity dependent absorption[31,32,35] seems to be in the favor of NLR. Previously we reported (i) electron dynamics,[31,32] (ii) harmonic emission,[36] and (iii) energy optimization[37] in clusters, mostly in the NLR regime. In this work, with self-consistent particle-in-cell (PIC) simulations as in Ref. 37, we report ion dynamics in further detail with 800 nm laser pulses of duration ≤23 fs (with FWHM ∼6 fs) where NLR is dominant. In particular, we show asymmetric Coulomb explosion of argon cluster in the NLR regime which is a topic of recent interest. The effect of NLR absorption of laser light by electrons on the inner ionization dynamics, cluster expansion, and the ion energy distribution was not addressed in greater detail in the earlier works.[31,32,36]

It was already mentioned that ionization ignition is responsible for higher charge states of cluster ions. With argon clusters we show that not all laser intensities lead to efficient ionization ignition. There can be "ionization depletion" (meaning that atoms inside the cluster are ionized to the charge states less than the isolated atoms in the gas phase) when laser field is strongly shielded by the space charge field in the cluster. However ions on the cluster boundary acquire higher charge states by the ionization ignition. The distribution of charge is shown to be symmetric in a plane (z–y plane) perpendicular to the direction (x-direction) of the

linearly polarized laser pulse, but asymmetric in the plane (x–y plane) of polarization. Moreover higher charge states exist along the direction of polarization (x-direction) than in the other two perpendicular directions. This asymmetric charge distribution already established at a shorter time (as considered in this work) may lead to the asymmetry of the ion kinetic energy seen in the rare-gas cluster experiments[5,7,38] where longer pulses were considered. Similar asymmetry was previously reported by classical Monte Carlo particle dynamics,[16] and molecular dynamics (MDS) (Ref. 39) simulations for rare-gas clusters with longer pulses. In those MD codes[39,40] and MD like codes,[16] due to Coulomb singularity, local decrease or increase of the field due to the neighboring electrons/ions may not be very accurate[16] which may lead to inaccurate charging of a cluster. In Ref. 39, the electric field of the neighboring ions was even *excluded* (probably to suppress the artificially high field due to the Coulomb singularity) which can have a pronounced effect on the inner ionization in the early stage of charging of the cluster (or during the short pulse duration) when ionic density is significantly high. The Coulomb singularity was mitigated by introducing a smoothing parameter r_s such that the actual distance between two particles $|r_j - r_i|$ was modified as $\sqrt{|r_j - r_i|^2 + r_s^2}$. This way electronic background was already shifted from the ionic background just after the optical field ionization (OFI). In Ref. 16, a new electron was placed with zero velocity shifted from its parent ion in the direction of the polarization of the laser field while in Refs. 14 and 39 the value of r_s was on the order of cluster radius R_0. Clearly an *asymmetry* was introduced in the electron configuration (which also lead to asymmetric Coulomb explosion) in the beginning itself (just after the OFI) by the way of electrons being placed. We emphasize that initial electron configuration is very important to justify asymmetric Coulomb explosion of a cluster. Here we use a different approach, namely PIC, which overcomes these difficulties. We start from a symmetric electron configuration after the OFI, and an asymmetry in the electron dynamics is introduced self-consistently (*even* without collision) by the laser field and the space-charge field that leads to asymmetric cluster expansion in spite of short laser pulses. Moreover, from Ref. 16 it appears that recombination plays an important role in the anisotropic distribution of ion energy. Instead, we show that this anisotropy may originate from a collisionless process with short pulses.

It is worth mentioning that experiments[41] with hydrogen clusters (where ionization ignition is absent) also showed asymmetry in the ion emission energies. Our results in this case (not reported here) indicate that the observed asymmetry is almost independent of the cluster type, since the spherical charge-symmetry of the system is initially broken by the asymmetric electron motion in a linearly polarized field. Recently, a new kind of asymmetry (i.e., higher ion yield perpendicular to the laser polarization direction than along the laser polarization direction) was reported in a few cluster experiments[42,43] which we have not yet found for the set of cluster and laser parameters of this work.

The paper is organized as follows. Section II describes necessary details of our PIC simulation. For argon clusters Sec. III shows ionization ignition with creation of higher charge states, asymmetric charge distribution and energy distribution of argon ions, and asymmetric cluster expansion. In Sec. IV, we summarize and conclude the results. Atomic units $\hbar = m = -e = 4\pi\varepsilon_0 = 1$ are used unless mentioned explicitly.

II. DETAILS OF THE PIC SIMULATION

First, we describe here the details of our three dimensional PIC simulations.[44] Additional details were mentioned in our earlier works.[31,32,36] A single cluster of radius R_0 and number of atoms N, is placed at the center of a computational box of volume Γ. Atoms are initially placed according to the Wigner-Seitz radius r_0 such that $R_0 = r_0 N^{1/3}$. For argon $r_0 = 0.24$ nm. In the present study R_0 is much smaller than λ (800 nm), and the skin depth $\lambda_{\rm skin} \equiv c/\omega_{\rm p}$ (c is the speed of light in vacuum, and $\omega_{\rm p}$ is the plasma frequency). Also the peak intensity of the laser pulse is chosen below 10^{18} Wcm^{-2}. It allows us to assume the dipole approximation $E_1(\boldsymbol{r}, t) = E_1(t)$ for the laser field.[14–16,36,37]

According to the Bethe rule[45] or over-the-barrier ionization of atoms, an electron is detached from a neutral atom of number of electrons Z and ionization potential $I_{\rm p}(Z)$ only when laser field satisfies

$$E_1(t) = I_{\rm p}^2(Z) Z^{-1}/4. \tag{1}$$

This is known as optical field ionization. We assume that all atoms are singly ionized (i.e., $Z = 1$) by the OFI. Soon after the OFI, laser field alters the charge equilibrium. Charges are mapped to the numerical grids and the Poisson's equation is solved for the potential $\Phi_G(x, y, z, t)$ on the grids with time dependent monopole boundary condition (discussed in the end of this section). Interpolating $\Phi_G(x, y, z, t)$ to a particle location $\boldsymbol{r}_i$ ($\boldsymbol{R}_i$ for ions), the potential $\Phi(\boldsymbol{r}_i, t)$ and the space charge field $\boldsymbol{E}_{\rm sc}(\mathrm{r}_i, t) = -\nabla\Phi(\boldsymbol{r}_i, t)$ are computed at individual particle locations $\boldsymbol{r}_i$. For large clusters, the space charge field $|\boldsymbol{E}_{\rm sc}(\boldsymbol{R}_i, t)|$ at the ion position $\boldsymbol{R}_i$ may immediately exceed $E_1(t)$ by many-fold and the total field $\boldsymbol{E}(\boldsymbol{R}_i, t) = \boldsymbol{E}_1(t) + \boldsymbol{E}_{\rm sc}(\boldsymbol{R}_i, t)$ can produce even higher charge states ($Z > 1$) of ions. Higher charge states ($Z > 1$) are created when the instantaneous total field $E(\boldsymbol{R}_i, t) = |\boldsymbol{E}(\boldsymbol{R}_i, t)|$ satisfies

$$E(\boldsymbol{R}_i, t) = I_{\rm p}^2(Z) Z^{-1}/4. \tag{2}$$

Additional effects such as collision of hot electrons with ions can also lead to collisional inner ionization. The latter needs electrons to be removed from the cluster and driven back to the ions by the laser field. Before the electrons are back-scattered to the ions, the ignition field $|\boldsymbol{E}_1(t) + \boldsymbol{E}_{\rm sc}(\boldsymbol{R}_i, t)|$ can become moderately higher to create highly charged ions. In Refs. 16 and 46, the contribution of collisional ionization was reported to be less than 2% compared to the over-the-barrier ionization even for bigger clusters with pulse lengths >100 fs which contradicts Ditmire's

nanoplasma model[22] where collisions were assumed to be the main mechanism behind the ionization and heating of a laser-driven cluster. Here, we neglect collisional effects and consider only collisionless case. Mobile ions are considered. New electrons are born with the same velocities and positions of the respective parent ions.

We use open boundary condition for the PIC particles so that the electrons which leave the simulation box may be driven back inside the box by the laser field at a later time. As long as a PIC electron is inside the computational box, the field at its location $\boldsymbol{r}_i(t)$ is $\boldsymbol{E}(\boldsymbol{r}_i,t) = \boldsymbol{E}_l(t) + \boldsymbol{E}_{sc}(\boldsymbol{r}_i,t)$. Outside the box $\boldsymbol{E}(\boldsymbol{r}_i,t) = \boldsymbol{E}_l(t)$ is assumed due to inappreciable $\boldsymbol{E}_{sc}(\mathrm{r}_i,t)$. The size of the simulation box is chosen as $2R_b$ with $R_b \simeq 16R_0$. A PIC electron (having same charge to mass ratio $e/m = -1$ as a real electron) satisfies the equation,

$$\ddot{\boldsymbol{r}}_i + \boldsymbol{E}_{sc}(\boldsymbol{r}_i,t) = -\boldsymbol{E}_l(t). \tag{3}$$

Equation of motion of j-th PIC ion of mass M reads

$$M\ddot{\boldsymbol{R}}_j - \boldsymbol{E}_{sc}(\boldsymbol{R}_j,t) = \boldsymbol{E}_l(t). \tag{4}$$

On the boundary R_b of the computational box the potential $\Phi_b(R_b,t)$ satisfies monopole potential $\Phi_b(R_b,t) = \int_\Gamma[\rho(x,y,z,t) - \rho_e(x,y,z,t)]d\Gamma/R_b$ which varies with the ionic charge density $\rho(x,y,z,t)$ and the electronic charge density $\rho_e(x,y,z,t)$ within the computational box. After each time step the above steps are repeated until the end of the applied laser pulse.

In this work we consider a single Ar_N cluster with number of atoms $N = 17\,256$. After the initial ionization by OFI, there are 128 particles/cell (including equal number of ions and electrons) with uniform cell size $\Delta = 32$ a.u., and number of cells 128^3. We choose a time step $\Delta t = 0.2$ a.u. (550 steps in one laser period) to ensure negligible artificial numerical heating.

III. RESULTS

We present results for an Ar_N cluster of radius $R_0 = 6.2$ nm and of number of atoms $N = 17256$ with a linearly polarized (along x-direction), $n = 8$ cycle $\sin^2$-laser pulses $E_l(t) = E_0 \sin^2(\omega_l t/2n)\cos(\omega_l t)$ of wavelength $\lambda_l = 800$ nm, but of various peak laser intensities I_0. The total pulse duration is 23 fs with FWHM ~6 fs. Depending upon the value of I_0, ions of different charge states are self-consistently produced during the pulse. Simultaneously cluster expansion, outer ionization and energy absorption by electrons also take place.

A. Inner ionization

Figures 1(a) and 1(b) show charge states vs the position (in units of R_0) of various ions through the cuts in x–y and y–z planes through the cluster center after the laser pulse (at $t = 23$ fs) of intensity 2.5×10^{14} Wcm^{-2}. At this intensity OFI (1) can create only the ionic charge state $Z = 1$. However it is observed that ions with $Z = 2$, 3 are also created which indicates a clear "ionization ignition."[11–19] During the pulse, displacement of electron cloud from the ionic background causes local charge imbalance which is maximum at the cluster ends along x (along the laser polarization) and comparatively lesser in the y and z-directions. As a result, higher value of $|\boldsymbol{E}_{sc}(\boldsymbol{R}_i,t)|$ is transiently developed at the cluster ends along x than at the ends along y and z. This can explain the origin of higher ionic charge along the direction of laser polarization in Fig. 1(a). Further charge asymmetry of the ions (sitting opposite to the center of the cluster) along the laser polarization in Fig. 1(a) is due to the unequal field amplitudes $|E_l(t) + E^x_{sc}(\boldsymbol{R}_i,t)|$ and $|E_l(t) - E^x_{sc}(\boldsymbol{R}_i,t)|$ during the pulse. However $|\boldsymbol{E}_{sc}(\mathrm{R}_i,t)|$ is symmetric in the y, z directions, generating a symmetric charge distribution of ions along those directions [see Fig. 1(b)].

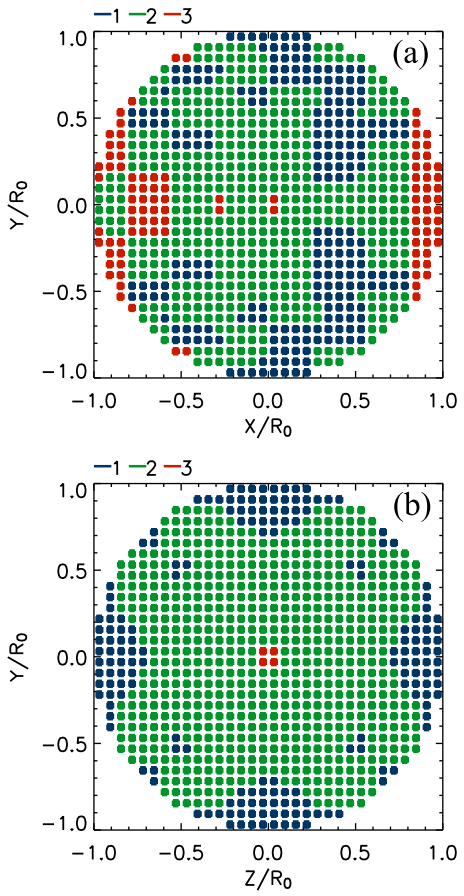

FIG. 1. Charging of Ar_{17256} cluster of radius $R_0 = 6.2$ nm at a laser intensity 2.5×10^{14} Wcm^{-2} and an $n = 8$ cycle laser pulse $E_l(t) = E_0 \sin^2(\omega_l t/2n)\cos(\omega_l t)$. (a) Projection of ion charge states at various ion positions in the x–y plane nearest to the $z = 0$ plane (seen through z-axis). (b) Projection of the ion charge states in the y–z plane nearest to the $x = 0$ plane (seen through x-axis). Ion positions are shown in units of initial radius R_0 at time $t = 23$ fs.

To see when those charge states were created during the laser pulse of intensity 2.5×10^{14} Wcm^{-2}, in Fig. 2 we plot laser field E_l (dotted line), total field $|\boldsymbol{E}_l(t) + \boldsymbol{E}_{sc}(\boldsymbol{R}_i,t)|$ (dotted-dashed lines) for different ions vs the laser cycles. Dashed lines represent the field strengths required for the creation of charge states $Z = 1$, 2, 3 according to OFI. All ions are charged to $Z = 1$ due to the OFI when laser field is maximum at 4-cycle (shown as single dot on the dashed line with $Z = 1$). After the 4-cycle, although laser field amplitude decreases, ions with charge $Z = 2$, 3 (successive dots on

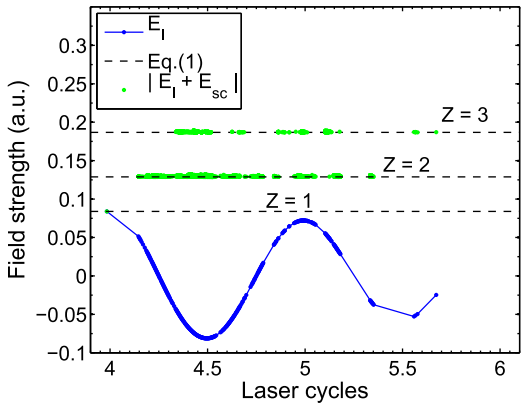

FIG. 2. Field strength vs the laser cycles at different ions corresponding to the cluster of radius $R_0 = 6.2$ nm in Fig. 1. Laser field E_l [line with dots (blue)] meets the required field strength (dashed line with $Z = 1$) according to the OFI Eq. (1) only at 4-cycle when all ions assume charge $Z = 1$. Total field $|\boldsymbol{E}_l(t) + \boldsymbol{E}_{sc}(\boldsymbol{R}_i, t)|$ at different ions exceeds [shown with dots (green)] laser field and produce ions of $Z = 2$, 3 after the 4-cycle when required field (Eq. (2), dashed lines with $Z = 2$, 3) is met.

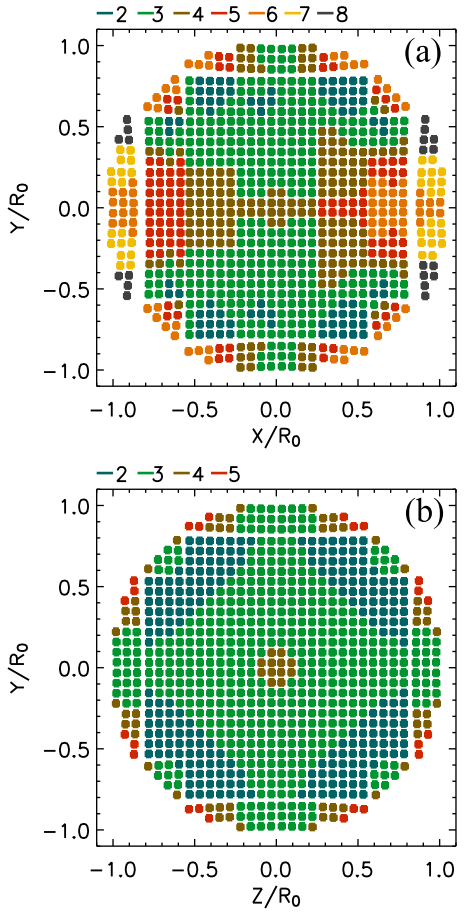

FIG. 3. (a) Projection of ion charge states at various ion positions in the $x-y$ plane nearest to the $z = 0$ plane (seen through z-axis). (b) Projection of the ion charge states in the $y-z$ plane nearest to the $x = 0$ plane (seen through x-axis). Maximum charge state $Z = 8$ is observed. Ion positions are shown in units of radius $R_0 = 6.2$ nm at time $t = 23$ fs. The laser intensity is 2.5×10^{15} Wcm^{-2}. Other parameters are same as in Fig. 1.

$Z = 2$, 3 dashed lines) are produced from $t \approx 4.145$-cycle and $t \approx 4.337$-cycle onwards. It is clearly seen that field amplitudes $|\boldsymbol{E}_l(t) + \boldsymbol{E}_{sc}(\boldsymbol{R}_i, t)|$ at different times are compatible with the charges states $Z = 1$, 2, 3 and the respective required field strengths according to Eq. (2).

Figures 3(a) and 3(b) show further evidence of the ionization ignition at an intensity 2.5×10^{15} Wcm^{-2}. Results are plotted in those planes explained in Figs. 1(a) and 1(b), respectively, at time $t = 23$ fs. In Fig. 3(a) highest charge state $Z = 8$ is visible at the cluster ends along the laser polarization in addition to the lower charge states $Z = 7$ to 2 toward the center. Figure 3(b) shows symmetric charge distribution of ions in the z–y plane as explained before. One does not see charge states $Z > 5$ in the z–y plane due to the absence of the laser field components in this plane. In the pure atomic case, charge states $Z < 4$ are only conceivable at this intensity according to the Bethe formula (1). Required ionization energy to produce Ar^{8+} is 5.3 a.u., i.e., an order of magnitude higher laser intensity $\approx 2.6 \times 10^{16}$ Wcm^{-2} is required. It helps to conclude that the higher charges $Z = 4$ to 8 are due to the "ionization ignition." Note that, ions with higher Z values ($Z = 6$, 7, 8, for this case) are primarily produced at the two ends of the cluster along the laser polarization. Relatively higher Coulomb repulsion between these ions causes their fast disintegration along the laser polarization from the rest which is visible in Fig. 3(a) whereas it is less pronounced in the z–y plane in Fig. 3(b). As a result of this, spherical symmetry of the ionic background is broken and the highly charged ions in the laser polarization expands much faster than the ions having less charge in the other directions. This is the reason why experimentally one gets asymmetric ion expansion[5,7,38] that originates due to the asymmetric charge distribution.

To know the variation of "ionization ignition" with laser intensity, the same cluster is illuminated with intensities $2.5 \times 10^{14} - 7.5 \times 10^{17}$ Wcm^{-2}. Figure 4 shows the maximum charge state Z_{max}, minimum charge state Z_{min}, average charge state Z_{av} (defined as the total charge of the cluster divided by the number of ions N) and the charge states predicted by the Bethe formula (1) of pure atomic ionization case vs the laser intensity, at the end of the laser pulse. The ratio Z_{max}/Z_{min} is also included in the plot. The highest value of $Z = 8$ in Fig. 3 indicates that the outer most shell ($3s^2 3p^6$) is completely ionized for those atoms. Ionization of the next inner atomic shell ($2s^2 2p^6$) of an argon atom and creation of charge states $Z > 9$ would require much higher field strength than in Fig. 3. This is possible either by increasing space charge field with bigger cluster size or by increasing the laser field strength. For the above cluster, if we increase the laser intensity further the highest charge state at the cluster boundary does not increase immediately but more and more ions from the boundary of the cluster to the center of the cluster achieve higher charge states with $Z < 8$. This is clearly visible in Fig. 4 between laser intensities 2.5×10^{15} Wcm$^{-2} - 10^{17}$ Wcm^{-2} where $Z_{max} = 8$ remains unchanged but Z_{av} increases. When compared with the pure atomic case, one would expect all ions to be $Z = 8$ at the intensity 10^{17} Wcm^{-2}. Instead we also see lower charge states $Z = 7 \rightarrow 3$ for some ions toward the center of the cluster. As a result, Z_{av} remains below the Z values predicted by the Bethe formula (1). We call it "ionization depletion" where space charge field counteracts to the laser

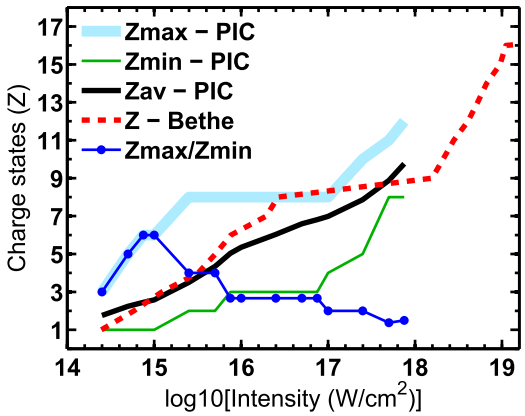

FIG. 4. Maximum ion charge Z_{max} (thick solid line), minimum ion charge Z_{min} (thin solid), average ion charge Z_{av} (bold black line), and the ion charge predicted by the Bethe rule (1) (dashed line) versus peak laser intensities for the cluster of radius $R_0 = 6.2$ nm in Fig. 1 with an $n = 8$ cycle laser pulse $E_l(t) = E_0 \sin^2(\omega_l t/2n)\cos(\omega_l t)$. Results are plotted at time $t = 23$ fs. Other parameters are same as in Fig. 1.

field (i.e., shielding of the laser field). At the next higher intensity 2.5×10^{17} Wcm^{-2} the maximum charge state seen in Fig. 4 is $Z = 10$ which requires an order of higher intensity $\approx 2.1 \times 10^{18}$ Wcm^{-2} in the pure atomic case. This shows that "ionization ignition" begins to play again after the intensity 10^{17} Wcm^{-2} with sharp increase in Z_{max}, Z_{min}, and Z_{av}.

From the above described scenario it is clear that "ionization ignition"is the mechanism by which cluster ions achieve the charge states higher than the pure atomic ionization case at a given laser intensity. Also there are higher laser intensities at which "ionization ignition" saturates due to the higher binding potential of the inner atomic shells. Close to those saturation intensities, "ionization depletion" works due to the shielding of the laser field by the space charge field in a sense opposite to that of the "ionization ignition." Not all intensities are useful for the efficient inner ionization of clusters. The maximum charge state Z_{max} mainly appears at the cluster boundary while the minimum charge state Z_{min} appears at the cluster center. The ionization model presented in Ref. 47, with Xenon cluster, predicted the ratio Z_{max}/Z_{min} to be between 1.5 and 2. Our results agree with this predicted value above the intensity 10^{16} Wcm^{-2}, but exceed the value $1.5 - 2$ for the intensities below 10^{16} Wcm^{-2} (see Fig. 4) where ionization ignition is very efficient.

B. Charge states and energy distribution of ions

Due to the mutual repulsion between the ions they start gaining energy during the pulse. For the above Ar_{17256} cluster, Figs. 5(a) and 5(b) show the charge states and the kinetic energies carried by different ion population N_{ion} just after the end of the laser pulses (i.e., at time 23 fs) of peak intensities 10^{17} Wcm^{-2} and 7.5×10^{17} Wcm^{-2}, respectively. From Fig. 5(a) it is observed that ions with $Z_{max} = 8$ are only driven with appreciable kinetic energies up to 25 keV while the rest (up to $Z_{min} = 4$) remains cold. At a higher laser intensity 7.5×10^{17} Wcm^{-2}, Fig. 5(b) shows the ions with $Z_{max} = 12$ and $Z_{min} = 8$. Unlike the results in Fig. 5(a), Fig. 5(b) shows that all ions are driven with higher kinetic

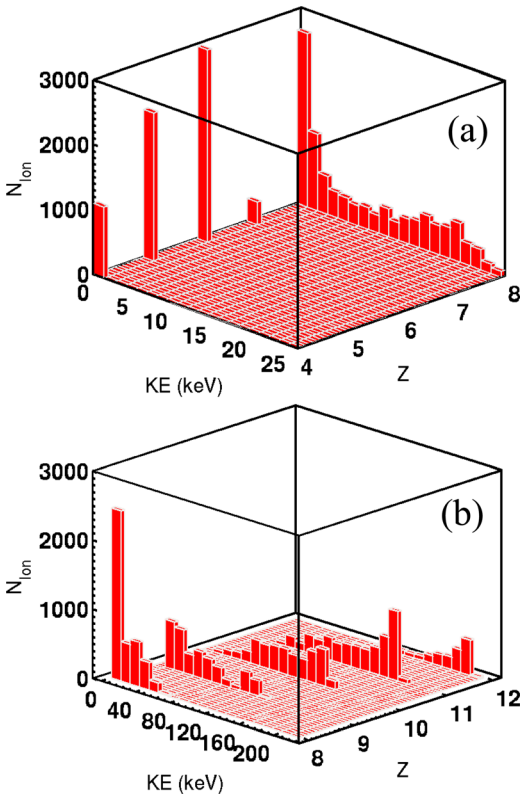

FIG. 5. Kinetic energy and charge (Z) distribution of ions for the Ar_{17256} cluster of radius $R_0 = 6.2$ nm in Fig. 1 for peak intensities (a) 10^{17} Wcm^{-2} and (b) 7.5×10^{17} Wcm^{-2} at a time $t = 23$ fs. Other parameters are same as in Fig. 1.

energies from 40 keV (with $Z_{min} = 8$) to 210 keV (with $Z_{max} = 12$). It should be noted that at higher values of the peak laser intensity OFI (also "ionization ignition") occurs at earlier laser cycles than at lower intensities. Therefore, with increasing peak laser intensity, onset of the ion motion takes place in the early laser cycles. If ions are followed even after the laser pulse, potential energy of the cluster will be converted totally to the kinetic energy of ions and the final kinetic energy of the ion fragments will be much higher than those are shown in Figs. 5(a) and 5(b). It can be seen that only the ions with the maximum charge states Z_{max} carry the maximum energy at a given laser intensity.

We cannot infer the anisotropic nature of energy distribution from Fig. 5. To identify it in detail, the distribution of total kinetic energy, x, y, and z-components of the kinetic energy of the different ion population N_{ion} are shown in Figs. 6(a) and 6(b) corresponding to Figs. 5(a) and 5(b), respectively. It is seen that ions have higher kinetic energy along the laser polarization (the x-component) than in the transverse directions (in the y, z-directions). Moreover, the y, z-components of energy are exactly same. The asymmetry in the energy distribution is due to the asymmetry in the charge distribution which is already seen in Fig. 3. With longer laser pulses, similar asymmetry in the ion energy distribution was observed in the rare-gas cluster experiments[5,7,38] and also reported with MD simulations of clusters.[16,39] However, from Refs. 16 and 39, it appears that collision[39] and recombination[16] play major role in the anisotropic distribution of ion

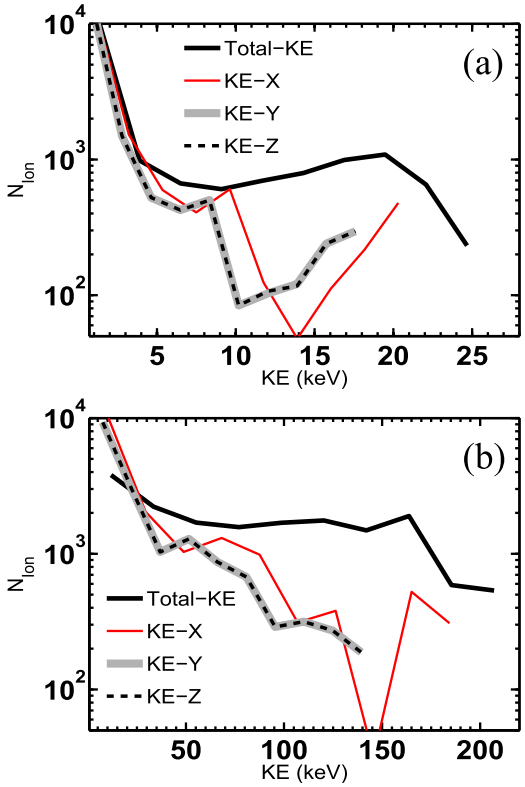

FIG. 6. Kinetic energy distribution of ions for the Ar_{17256} cluster of radius $R_0 = 6.2$ nm in Fig. 1 for peak intensities (a) 10^{17} Wcm^{-2} and (b) 7.5×10^{17} Wcm^{-2} at time $t = 23$ fs. It shows asymmetric kinetic energy distribution. Other parameters are same as in Fig. 1.

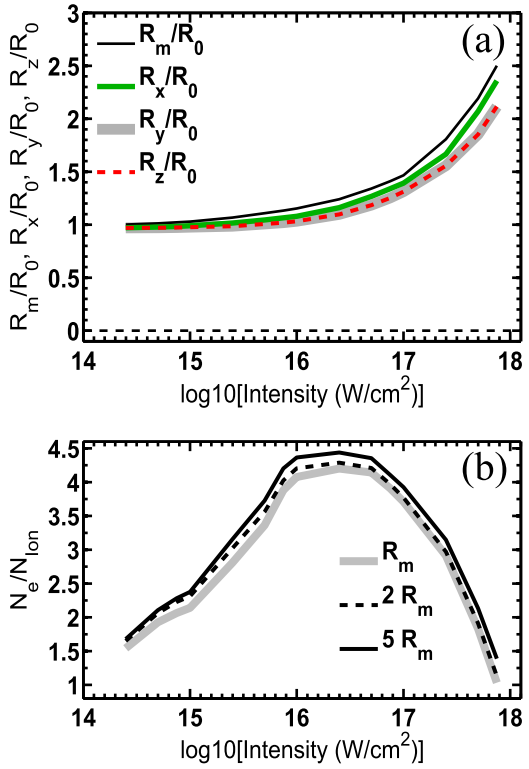

FIG. 7. (a) Normalized expansion radius R_x/R_0 along the laser polarization (x–direction), $R_y/R_0, R_z/R_0$ (along y, z), and the average radius $R_m/R_0 = \sqrt{R_x^2 + R_y^2 + R_z^2}/R_0$ of the cluster vs the peak intensity showing asymmetric expansion in position space. (b) Normalized electron number N_e/N_{ion} inside various R_m vs the peak intensity. Results are plotted at time $t = 23$ fs. Other parameters are same as in Fig. 6.

energy. With shorter pulses, we show that this anisotropy actually originates from a collisionless process.

C. Asymmetric cluster expansion

The origin of the energetic ions as described in Sec. III B is a consequence of the cluster expansion that largely depends upon the charge distribution of ions. For a homogeneous spherical charge distribution it is clear that expansion is uniform, i.e., any concentric layer in the cluster moves at the same speed of its outer boundary. In the realistic cluster expansion case, ions at different radial positions move outward with different speed due to the charge inhomogeneity (see Figs. 1 and 3).

The anisotropy in the energy distribution as seen in Fig. 6 should also be manifested in the radial expansion of the cluster. To show it clearly, Figure 7(a) shows the normalized expansion radius R_x/R_0 along the laser polarization, and $R_y/R_0, R_z/R_0$ perpendicular to the laser polarization direction, and the average radius $R_m/R_0 = \sqrt{R_x^2 + R_y^2 + R_z^2}/R_0$ vs the peak laser intensity. Results are plotted after the pulse, i.e., at time $t = 23$ fs. It is clear that cluster expands faster in the laser polarization direction (in x) than in the normal (y, z) direction. We can also infer that $R_y = R_z$, meaning expansion in y, z are symmetric for all peak intensities.

Expansion of the cluster also depends upon the number of electrons N_e those stays inside and in the immediate vicinity of the cluster. The inside electrons lowers the net positive charge and slows down the expansion. Figure 7(b) shows normalized electron number N_e/N_{ion} within different radii R_m, $2R_m$ and $5R_m$ after the pulse at various laser intensities. For a fixed radius, N_e/N_{ion} initially increases with increasing laser intensity due to pronounced "inner ionization" than the "outer ionization," reaches a maximum where "inner ionization" is balanced by the "outer ionization." After the maximum, situation is reversed, i.e., N_e/N_{ion} decreases with increasing intensity because "outer ionization" becomes more pronounced than the "inner ionization." At the intensity 10^{16} Wcm^{-2} one sees approximately $N_e/N_{ion} \approx 4$, i.e., $N_e \approx 69\,000$ electrons within the expanded cluster of radius R_m after the laser pulse. At a higher intensity 7.5×10^{17} Wcm^{-2} it decreases to the value $N_e/N_{ion} \approx 1$, i.e., $N_e \approx 17256$ electrons stay inside R_m. We shall use these information of N_e in Sec. III C 1.

1. Comparison with a homogeneously charged sphere model

From the above results it is intuitive that the expansion process of the cluster is in the favor of Coulomb expansion rather the hydrodynamic expansion which occurs in a longer time scale, typically >100 fs.[13,22] This can be justified by comparing our results with a simplified model[13] of the cluster expansion. According to this model a homogeneous

positively charged sphere (resembles with the ionic background) with total charge Q_p, radius R_0 and mass M_p expands electro-statically as

$$\ddot{R} = \frac{Q_p}{M_p R^2}. \quad (5)$$

$R(t)$ is the instantaneous radius. The solution of Eq. (5) with the initial conditions $R(t_{in}) = R_0$ and $\dot{R}(t_{in}) = 0$ reads

$$t = t_{in} + \sqrt{\frac{M_p R_0^3}{2Q_p^2}}\left(\sqrt{p^2 - p} + \log(\sqrt{p} + \sqrt{p-1})\right). \quad (6)$$

Here, t_{in} is the initial time and $p = R(t)/R_0$ is the ratio of the instantaneous radius to the initial radius of the cluster. This model does not consider the presence of electrons within the expanding cluster. Also it assumes that the total positive charge is constant (absence of inner ionization). In the realistic simulation (such as PIC or MD) part of the positive ion background may be compensated by the electrons if not all electrons leave the cluster at a certain time. During the pulse, inner ionization changes the total charge of the ionic background. With the increasing laser intensity, inner ionization as well as cluster expansion starts at lower value of t_{in}. In spite of these differences, Eq. (5) proves to be useful for understanding the cluster expansion to some extent. The use of the model Eq. (5) is not to show the anisotropic expansion. We want to show how the average radius $R_m(t) = \sqrt{R_x^2 + R_y^2 + R_z^2}$ of expansion obtained from PIC simulation (note that we shall represent $R_m(t)$ as $R(t)$ for convenience) compares with this symmetric expansion the model, so that from the deviation between the two we can justify the dominant expansion process. For the evolution of the Eq. (6), we require two input parameters: the net positive charge Q_p and the initial time t_{in}. The value of Q_p depends on the total positive charge and number of electrons N_e inside the cluster. From the PIC simulation the total ion charge $N_{ion}Z_{av}$ (see Fig. 4) and the number N_e [see Fig. 7(b)] after the laser pulse are explicitly known which allow us to assume $Q_p = N_{ion}Z_{av} - N_e$ at the initial time t_{in}. Note that t_{in} is different at a different peak laser intensity which is adjusted to the time when first electrons are removed from the atoms of the cluster according to the OFI (1).

Figures 8(a) and 8(b) show $R(t)/R_0$ vs time (in units of laser cycles) at different laser intensities, obtained from the PIC simulation and from the model (6) respectively. The results according to the model [in Fig. 8(b)] fit well with the PIC results [in Fig. 8(a)] at lower laser intensities $\leq 10^{17}$ Wcm^{-2}. At higher intensities $>10^{17}$ Wcm^{-2} expansion is much faster according to the model than the PIC results shown. This is due to the assumption of the constant value of the total charge Q_p and the absence of inner ionization in the model. In the PIC simulation, the bound electrons in the cluster potential will reduce the value of Q_p and a slower expansion is expected. We may further compare the time scale of expansion from the model (6). Let us assume that cluster is ionized at time $t_{in} = 0$. Then the required time

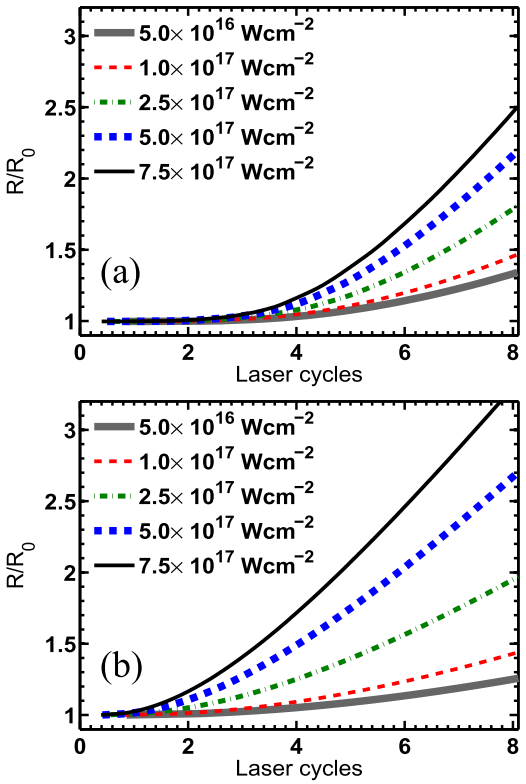

FIG. 8. Normalized radius $R(t)/R_0$ of the cluster of initial radius $R_0 = 6.2$ nm in Fig. 1 vs the laser cycles at different peak laser intensities with (a) PIC simulation and (b) with the model (5). Other parameters are same as in Fig. 1.

to double the cluster radius (setting $p = 2$) is $t = 1.6232\sqrt{M_i r_0^3}/Z$ (M_i being the mass of an argon atom). For argon it gives $t = (100.73/Z)$ fs, which shows that if the average charge Z is more in the cluster it take less time to double its radius. Considering the average charge $Z = 2-10$ from Fig. 4 for peak intensities $2.5 \times 10^{14} - 7.5 \times 10^{17}$ Wcm^{-2}, this expansion time may be found to vary from 50 fs to 10 fs. Our pulse duration of 23 fs, clearly lies in the regime of Coulomb expansion. From the comparison between PIC results and the model, it can be concluded that expansion of cluster is mainly due to the Coulomb repulsion by which highly charged ions are accelerated with higher kinetic energies as in Fig. 5.

IV. SUMMARY AND CONCLUSION

We presented results obtained by three-dimensional particle-in-cell simulations for argon clusters irradiated by near infrared, short laser pulses (<23 fs) where NLR plays a dominant role. In the present PIC simulations self-consistent development of ionic charges in the mean field produced by the charge particles (electrons and ions) and the laser field with mobile ions are considered. This enabled us to obtain various ionic outcome (e.g., ionic charge states and energies of different ions) of the short-pulse laser cluster interaction as opposed to the conventional long pulse scenario. Almost all features of the interaction, namely ion emission up to a few 100 keV energy, and higher charge state of argon ions along

the laser polarization than in the transverse directions, asymmetry in the ion energy distribution were obtained.

High charge states of the argon clusters were obtained due to the ionization ignition. However saturation of ionization ignition was found at laser intensities where laser field was shielded by the space charge field. Close to those saturation intensities average ionic charge (total charge divided by the number of atoms) is less than the atoms in the gas phase and "ionization depletion" occurs. Therefore, not all laser intensities are in favor of ionization ignition. Ionization depletion becomes stronger when there is a sharp jump in the binding potential of the cluster atoms, i.e., during the transition from one atomic shell to the next inner atomic shell of higher binding potential.

The maximum ion energies are carried mainly by the ions with higher charge states which appear on the outer cluster boundary along the laser polarization. Cluster expansion was compared with a Coulomb expansion model which showed ion expansion was mainly due to the Coulomb force between the cluster ions. The effect of hydrodynamic expansion was insignificant. The asymmetric Coulomb expansion shown in this work is due to collisionless absorption process. However results may vary in presence of collisions and other random processes.

ACKNOWLEDGMENTS

The author acknowledges Dieter Bauer for fruitful discussions, N. Ramasubramanian and S. Sengupta for careful reading of the manuscript.

APPENDIX: ANISOTROPIC ENERGY DISTRIBUTION OF IONS DUE TO COLLISIONAL IONIZATION

To see how the anisotropy changes with collisional ionization, we have performed PIC simulation with electron impact ionization (in addition to the ionization by the OFI and the space charge field) for an argon cluster of radius $R_0 = 3.11\,\text{nm}$ and number of atoms $N = 2176$. The same $\sin^2$-pulse $E_l(t) = E_0 \sin^2(\omega_l t/2n)\cos(\omega_l t)$ of peak intensity $2.5 \times 10^{14}\,\text{Wcm}^{-2}$ as in Fig. 1 is chosen with $n = 5$-cycles. The PIC simulation of a bigger cluster, including collision, being computationally very intensive we have chosen a smaller cluster and a shorter pulse duration than considered in Sec. III. The details of the collisional ionization will not be discussed here, for the sake of conciseness. Only the necessary results will be presented.

Figures 9(a) and 9(b) show the distribution of *x, y,* and *z*-components of the kinetic energy of the different ion population N_{ion} without the collisional ionization (as shown earlier in Fig. 6) and with the collisional ionization respectively. Results are plotted after the completion of the 5-cycle laser pulse, i.e., at a time $t \approx 14\,\text{fs}$. Asymmetric energy distributions are seen (in Fig. 9) for both the cases with *x*-components having higher values than the respective *y, z* components. The *y, z*-components of energy in Fig. 9(b) are not exactly the same as seen in Fig. 9(a) due to the random nature of the collisional ionization. In the process of collisional ionization, the projectile electrons loose energy and slow down. A fraction of electrons created by collisional ionization, and the old projectile electrons may stay inside the cluster or in its vicinity. As a result, the net repulsive force among the ions is weaker in Fig. 9(b) which leads to lower values of kinetic energy components compared to Fig. 9(a) at given laser intensity.

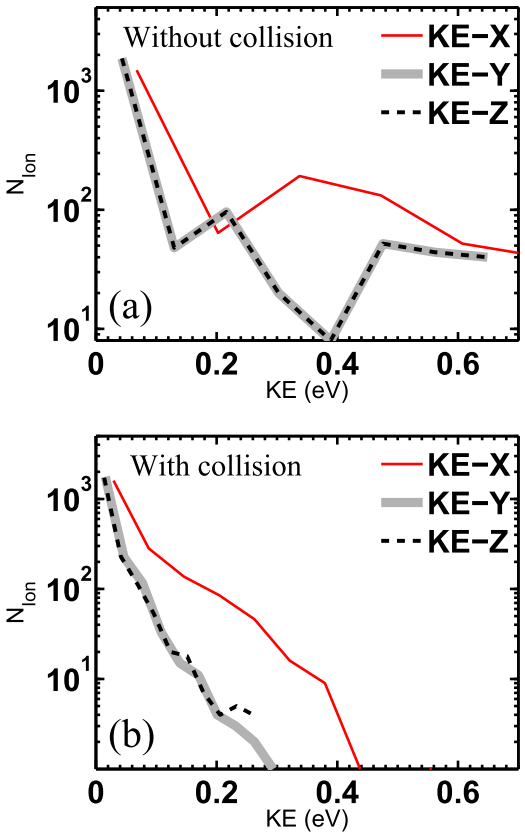

FIG. 9. Kinetic energy distribution of ions (similar to Fig. 6) from an argon cluster of radius $R_0 = 3.11\,\text{nm}$ and number of atoms $N = 2176$ with $n = 5$ cycle laser pulse $E_l(t) = E_0 \sin^2(\omega_l t/2n)\cos(\omega_l t)$ of peak intensity $2.5 \times 10^{14}\,\text{Wcm}^{-2}$ as in Fig. 1. Results are plotted after the laser pulse, i.e., at a time $t \approx 14\,\text{fs}$. It shows asymmetric kinetic energy distribution for both the cases: (a) without collisional ionization and (b) with collisional ionization.

For the above intensity, the ponderomotive energy $U_p = E_0^2/4\omega_l^2$ (i.e., the average energy of a free electron in a laser field) of an electron is only $\approx 14.9\,\text{eV}$ which is even less than the ionization potential $\approx 15.6\,\text{eV}$ of an argon atom corresponding to the charge state $Z = 1$. The higher impact energy which is required for the creation of the higher charge state $Z > 1$ is initially supplied to the projectile electron via the NLR. We conclude that collisional ionization does play role in the anisotropic explosion of a laser-driven cluster, but this anisotropy is originally created by the collisionless absorption processes–the NLR–by which an electron gains sufficient energy to collisionally ionize an ion in the later time.

[1]T. Ditmire, J. W. G. Tisch, E. Springate, M. B. Mason, N. Hay, J. Marangos, and M. H. R. Hutchinson, Nature (London) **386**, 54 (1997).
[2]T. Ditmire, R. A. Smith, J. W. G. Tisch, and M. H. R. Hutchinson, Phys. Rev. Lett. **78**, 3121 (1997).
[3]T. Ditmire, J. W. G. Tisch, E. Springate, M. B. Mason, N. Hay, J. P. Marangos, and M. H. R. Hutchinson, Phys. Rev. Lett. **78**, 2732 (1997).

[4]V. Kumarappan, M. Krishnamurthy, D. Mathur, and L. C. Tribedi, Phys. Rev. A **63**, 023203 (2001).
[5]M. Krishnamurthy, D. Mathur, and V. Kumarappan, Phys. Rev. A **69**, 033202 (2004); V. Kumarappan, M. Krishnamurthy, and D. Mathur, Phys. Rev. Lett. **87**, 085005 (2001).
[6]M. Krishnamurthy, J. Jha, D. Mathur, Ch. Jungreuthmayer, L. Ramunno, J. Zanghellini, and T. Brabec, J. Phys. B **39**, 625 (2006).
[7]M. Lezius, S. Dobosz, D. Normand, and M. Schmidt Phys. Rev. Lett. **80**, 261 (1998).
[8]V. Kumarappan, M. Krishnamurthy, and D. Mathur, Phys. Rev. A **66**, 033203 (2002).
[9]E. Springate, N. Hay, J. W. G. Tisch, M. B. Mason, T. Ditmire, M. H. R. Hutchinson, and J. P. Marangos, Phys. Rev. A **61**, 063201 (2000).
[10]E. Springate, S. A. Aseyev, S. Zamith, and M. J. J. Vrakking, Phys. Rev. A **68**, 053201 (2003).
[11]U. Saalmann and J. M. Rost, J. Phys. B **39**, R39–R77 (2006).
[12]Th. Fennel, K.-H. Meiwes-Broer, J. Tiggesbäumker, P.-G. Reinhard, P. M. Dinh, and E. Suraud, Rev. Mod. Phys. **82**, 1793 (2010).
[13]V. P. Krainov and M. B. Smirnov, Phys. Rep. **370**, 237 (2002).
[14]C. Rose-Petruck, K. J. Schafer, K. R. Wilson, and C. P. J. Barty, Phys. Rev. A **55**, 1182 (1997).
[15]D. Bauer and A. Macchi, Phys. Rev. A **68**, 033201 (2003).
[16]K. Ishikawa and T. Blenski, Phys. Rev. A **62**, 063204 (2000).
[17]F. Megi, M. Belkacem, M. A. Bouchene, E. Suraud, and G. Zwicknagel, J. Phys. B **36**, 273 (2003).
[18]C. Jungreuthmayer, M. Geissler, J. Zanghellini, and T. Brabec, Phys. Rev. Lett. **92**, 133401 (2004).
[19]D. Bauer, J. Phys. B **37**, 3085 (2004).
[20]C. Siedschlag and J. M. Rost, Phys. Rev. Lett. **93**, 043402 (2004).
[21]C. Jungreuthmayer, L. Ramunno, J. Zanghellini, and T. Brabec, J. Phys. B **38**, 3029 (2005).
[22]T. Ditmire, T. Donnelly, A. M. Rubenchik, R. W. Falcone, and M. D. Perry, Phys. Rev. A **53**, 3379 (1996).
[23]T. Döppner, Th. Fennel, Th. Diederich, J. Tiggesbäumker, and K. H. Meiwes-Broer, Phys. Rev. Lett. **94**, 013401 (2005).
[24]L. Köller, M. Schumacher, J. Köhn, S. Teuber, J. Tiggesbäumker, and K. H. Meiwes-Broer, Phys. Rev. Lett. **82**, 3783 (1999).
[25]S. Zamith, T. Martchenko, Y. Ni, S. A. Aseyev, H. G. Muller, and M. J. J. Vrakking, Phys. Rev. A **70**, 011201(R) (2004).
[26]I. Last and J. Jortner, Phys. Rev. A **60**, 2215 (1999).
[27]U. Saalmann and J.-M. Rost, Phys. Rev. Lett. **91**, 223401 (2003).
[28]Th. Fennel, G. F. Bertsch, and K. H. Meiwes-Broer, Eur. Phys. J. D **29**, 367 (2004).
[29]C. Siedschlag and J. M. Rost, Phys. Rev. A **71**, 031401 (2005).
[30]T. Martchenko, Ch. Siedschlag, S. Zamith, H. G. Muller, and M. J. J. Vrakking, Phys. Rev. A **72**, 053202 (2005).
[31]M. Kundu and D. Bauer, Phys. Rev. Lett. **96**, 123401 (2006).
[32]M. Kundu and D. Bauer, Phys. Rev. A **74**, 063202 (2006).
[33]P. Mulser and M. Kanapathipillai, Phys. Rev. A **71**, 063201 (2005); P. Mulser, M. Kanapathipillai, and D. H. H. Hoffmann, Phys. Rev. Lett. **95**, 103401 (2005).
[34]L. M. Chen, J. J. Park, K. H. Hong, I. W. Choi, J. L. Kim, J. Zhang, and C. H. Nam, Phys. Plasmas **9**, 3595 (2002).
[35]T. Taguchi, T. M. Antonsen, Jr., and H. M. Milchberg, Phys. Rev. Lett. **92**, 205003 (2004); T. M. Antonsen, Jr., T. Taguchi, A. Gupta, J. Palastro, and H. M. Milchberg, Phys. Plasmas **12**, 056703 (2005).
[36]M. Kundu, S. V. Popruzhenko, and D. Bauer, Phys. Rev. A **76**, 033201 (2007); S. V. Popruzhenko, M. Kundu, D. F. Zaretsky, and D. Bauer, Phys. Rev. A **77**, 063201 (2008).
[37]M. Kundu and D. Bauer, Phys. Plasmas **15**, 033303 (2008).
[38]M. Hirokane, S. Shimizu, M. Hashida, S. Okada, S. Okihara, F. Sato, T. Iida, and S. Sakabe, Phys. Rev. A **69**, 063201 (2004).
[39]A. R. Holkundkar, G. Mishra, and N. K. Gupta, Phys. Plasmas **18**, 053102 (2011).
[40]G. M. Petrov, J. Davis, A. L. Velikovich, P. Kepple, A. Dasgupta, and R. W. Clark, Phys. Plasmas **12**, 063103 (2005).
[41]D. R. Symes, M. Hohenberger, A. Henig, and T. Ditmire, Phys. Rev. Lett. **98**, 123401 (2007).
[42]E. Skopalová, Y. C. El-Taha, A. Zaïr, M. Hohenberger, E. Springate, J. W. G. Tisch, R. A. Smith, and J. P. Marangos, Phys. Rev. Lett. **104**, 203401 (2010).
[43]D. Mathur, F. A. Rajgara, A. R. Holkundkar, and N. K. Gupta, Phys. Rev. A **82**, 025201 (2010).
[44]C. K. Birdsall and A. B. Langdon, *Plasma Physics via Computer Simulation* (IOP, Bristol, 1991).
[45]H. A. Bethe and E. E. Salpeter, *Quantum Mechanics of One- and Two-Electron Atoms* (Plenum Publishing Corporation, New York, 1977).
[46]I. Last and J. Jortner, Phys. Rev. A **62**, 013201 (2000).
[47]M. B. Smirnov and V. P. Krainov, Phys. Rev. A **69**, 043201 (2004).